DRAM1 requires PI(3,5)P_2 generation by PIKfyve to deliver vesicles and their cargo to endolysosomes

Michiel van der Vaart*, Adrianna Banducci-Karp, Gabriel Forn-Cuní, Philip M. M. Witt, Joost J. Willemse, Salomé Muñoz Sánchez, Rohola Hosseini, Annemarie H. Meijer*

Animal Sciences, Institute of Biology Leiden, Leiden University, Leiden, 2333CC, The Netherlands

*Corresponding authors:
Michiel van der Vaart (m.van.der.vaart@biology.leidenuniv.nl)
Annemarie Meijer (a.h.meijer@biology.leidenuniv.nl)

Abstract (150 / 150 words)

Endolysosomal vesicle trafficking and autophagy are crucial degradative pathways in maintenance of cellular homeostasis. The transmembrane protein DRAM1 is a potential therapeutic target that primarily localises to endolysosomal vesicles and promotes autophagy and vesicle fusion with lysosomes. However, the molecular mechanisms underlying DRAM1-mediated vesicle fusion events remain unclear. Using high-resolution confocal microscopy in the zebrafish model, we show that mCherry-Dram1 labelled vesicles interact and fuse with early endosomes marked by PI(3)P. Following these fusion events, early endosomes mature into late endosomes in a process dependent on the conversion of PI(3)P into PI(3,5)P_2 by the lipid kinase PIKfyve. Chemical inhibition of PIKfyve reduces the targeting of Dram1 to acidic endolysosomal vesicles, arresting Dram1 in multivesicular bodies, early endosomes, or non-acidified vesicles halted in their fusion with early endosomes. In conclusion, Dram1-mediated vesicle fusion requires the formation of PI(3,5)P_2 to deliver vesicles and their cargo to the degradative environment of the lysosome.

Introduction

Endocytic processes are specialised in the uptake of substances from the microenvironment of the cell. Although most of the endocytic cargo is used for cellular sustenance or recycled back to the plasma membrane, a proportion of endocytosed material (e.g. pathogens and remnants of dead cells) is routed towards acidic and hydrolytic lysosomes for its degradation (Huotari and Helenius, 2011). While the endolysosomal system is responsible for degradation of unwanted extracellular material, autophagy performs a similar housekeeping function for the removal of intracellular material. During autophagy, cytoplasmic content is captured in double membraned vesicles and delivered to the endolysosomal system for degradation and recycling (Glick et al., 2010). In this way, autophagy replenishes nutrient levels in times of cellular starvation, and clears the cytoplasm of unwanted elements like protein aggregates, malfunctioning organelles, and intracellular pathogens (Saha et al., 2018). Routing endosomal and autophagosomal content to the degradative environment of the lysosome requires multiple vesicle fusion and maturation steps. Disruptions in these processes can result in serious pathologies, including neurodegenerative diseases, lysosomal storage disorders, infection, and cancer (Cossart and Helenius, 2014; Deretic et al., 2013; Malik et al., 2019; Sun, 2018; Tzeng and Wang, 2016).

DNA damage regulated autophagy modulator 1 (DRAM1) regulates autophagy and endolysosomal fusion events. DRAM1 was first identified as a cellular stress-induced regulator of autophagy and cell death downstream of tumour suppressor protein p53 (Crighton et al., 2006). DRAM1 primarily localises to lysosomes but can also be detected on other organelles of the vesicular trafficking system, including endosomes, autophagosomes, autolysosomes, the Golgi apparatus, and the endoplasmic reticulum (Crighton et al., 2006; Mah et al., 2012). Furthermore, DRAM1 was found to regulate fusion between autophagosomes and lysosomes, a process called autophagic flux (Zhang et al., 2013). When

host cells detect pathogenic mycobacteria that cause tuberculosis, *DRAM1* expression is activated downstream of the immunity regulating transcription factor NFκB (van der Vaart et al., 2014). Knockdown or knockout of *dram1* increased susceptibility to mycobacterial infection in zebrafish, identifying Dram1 as a host resistance factor (van der Vaart et al., 2014; Zhang et al., 2020). In support of this finding, overexpression of *dram1* was protective against mycobacterial infection by enhancing autophagic defences against intracellular bacteria and stimulating vesicle fusion events with lysosomes (van der Vaart et al., 2014). Although the effects of DRAM1 activation on autophagy and endolysosomal fusion events are described for several situations, its underlying molecular function in these processes remains unknown.

Endocytic cargo is sorted in early endosomes marked by the GTPase Rab5 (Zerial and McBride, 2001). Early endosomes containing cargo destined for degradation gradually replace Rab5 on their membrane for Rab7, while lowering their luminal pH from values above pH 6 to pH 6.0-4.9 to become late endosomes (Maxfield and Yamashiro, 1987; Zerial and McBride, 2001). During this phase of the maturation process, the outer endosomal membrane starts budding inwards to form intraluminal vesicles (Raiborg et al., 2002; Sachse et al., 2002). The resulting multivesicular bodies are a type of late endosome that also receive cargo destined for degradation by fusing with autophagosomes (Fader and Colombo, 2009). Late endosomes then undergo transient 'kiss-and-run' interactions with lysosomes, before eventually undergoing full fusion with lysosomes to reach the endpoint of this degradative pathway at a luminal pH of around 4.5 (Maxfield and Yamashiro, 1987). This process of endolysosomal maturation is extensively reviewed by Huotari & Helenius (Huotari and Helenius, 2011).

The identity of endolysosomal vesicles is in part determined by the presence of phosphoinositide (PI) lipids in their membrane that serve as docking sites for effector proteins (Hammond et al., 2012; Heo et al., 2006; Strahl and Thorner, 2007). PIs can be phosphorylated and dephosphorylated on the hydroxyl groups at the three, four, and five positions of their inositol rings by a range of kinases and phosphatases, generating a total of 7 different PIs in animals (Banerjee and Kane, 2020). Typically, early endosomes are defined by the presence of PI(3)P in their membrane, which is converted into PI(3,5)P_2 by the lipid kinase PIKfyve (Fab1p in yeast) during maturation into late endosomes (Wallroth and Haucke, 2018). Deletion or inhibition of PIKfyve/Fab1p results in accumulation of enlarged early/late hybrid endosomes that contain few intraluminal vesicles (Cai et al., 2013; Futter et al., 2001; Ikonomov et al., 2003; Jefferies et al., 2008; Odorizzi et al., 1998).

To gain a better understanding of the mechanisms behind DRAM1-mediated vesicle fusion events, we used the zebrafish *in vivo* model to study the potential link between DRAM1 and PI lipids involved in endolysosomal fusion and maturation. By generating a transgenic line that ubiquitously expresses fluorescently-tagged Dram1, we were able to confirm that Dram1 primarily localises to acidic vesicles. High-resolution confocal time-lapse imaging revealed that fluorescently-tagged Dram1 labels dynamic vesicles that display either a globular or tubular morphology. These Dram1-positive vesicles interact and fuse with early endosomes containing PI(3)P in their membranes. Early endosomes that have fused with Dram1-positive vesicles mature into late endosomes as they gradually reduce the presence of PI(3)P lipids in their membranes. Inhibition of PIKfyve, which prevents the formation of PI(3,5)P_2, reduced the targeting of Dram1 to acidic endolysosomal vesicles (late endosomes and lysosomes). Instead, fluorescently-tagged Dram1 accumulated in multivesicular bodies, early endosomes, and non-acidified vesicles halted in their fusion with early endosomes. Based on these findings, we conclude that Dram1-mediated vesicle fusion is dependent on the formation of PI(3,5)P_2 by PIKfyve to deliver vesicles and their cargo to the degradative environment of the lysosome.

Results

mCherry-Dram1 labels vesicles that interact and fuse with early endosomes

The molecular function of DRAM1 in vesicle trafficking remains largely unknown. To understand the breadth of it's possible functions, we used the Eukaryotic Linear Motif (ELM)(Kumar et al., 2020) resource to predict functional sites in the human DRAM1 protein (Figure 1A). This analysis confirmed the previously reported presence of 6 transmembrane domains (Crighton et al., 2006), suggesting that DRAM1 is embedded in cellular membranes with parts of the protein exposed to opposite sides of this membrane. Amongst the predicted protein domains, we identified two domains that support a function for DRAM1 in vesicle trafficking. Eps15 homology (EH) domains are generally present in proteins that regulate endocytosis or vesicle trafficking processes (Naslavsky and Caplan, 2005). The autophagy-related protein Atg8 and its homologs LC3 and GABARAP are markers of autophagosomes (Glick et al., 2010). The presence of Atg8 interacting domains therefore suggests that DRAM1 can interact with the autophagy-machinery.

We aimed to study the dynamic localisation of DRAM1 during endolysosomal maturation processes. For this purpose, we used a previously described mCherry-Dram1 construct under control of the ubiquitous beta actin promoter to generate a transgenic zebrafish line fluorescently reporting the subcellular localisation of Dram1 (van der Vaart et al., 2014), named Tg(*bactin:mCherry-dram1*). We could readily trace mCherry-Dram1 over time by confocal imaging epithelial cells in the thin tissue of the tail fin of 3 days post fertilisation (dpf) zebrafish larvae (Figure 1B and C). Time-lapse imaging revealed that mCherry-Dram1 labels motile and morphologically diverse globular and tubular vesicles (Figure 1C, Supplementary movie 1). We used a LysoTracker probe that accumulates and fluoresces in endolysosomal compartments with low luminal pH to confirm that mCherry-Dram1 mainly localises to these acidic organelles (Figure 1D). Previously we have demonstrated that ectopic activation of Dram1 by means of mRNA overexpression increased the number of autophagosomes observed per cell, and that transiently expressed mCherry-Dram1 can interact with autophagosomes (van der Vaart et al., 2014). To confirm that the mCherry-Dram1 construct retains the function of the endogenous protein, we crossed heterozygous *Tg(bactin:mCherry-dram1)* animals with the autophagy reporter line *Tg(CMV:GFP-Lc3)* (He et al., 2009). Co-expression of these two transgenes confirmed that mCherry-Dram1 interacts with autophagosomes and that ectopic expression of mCherry-Dram1 increased the number of autophagosomes observed per cell (Figure S1A and B). We can therefore use artificial expression of mCherry-Dram1 as a gain-of-function approach to study the role of Dram1 in vesicle trafficking.

To visualise endosomal vesicles that Dram1 interacts with, we used a transgenic line that fluorescently reports early endosomes in basal cell layer epithelial cells of the zebrafish epidermis: *TgBAC(ΔNp63:Gal4FF)*^{la213}; *Tg(4xUAS:EGFP-2xFYVE)*^{la214}, hereafter referred to as GFP-2xFYVE (Rasmussen et al., 2015). The GFP-2xFYVE probe incorporates specifically in membranes containing PI(3)P via its FYVE domains, thereby labelling early endosomes. However, a specific pool of PI(3)P also labels (nascent) autophagosomes (Nascimbeni et al., 2017). We therefore first tested the specificity of the GFP-2xFYVE probe by combining it with a *Tg(bactin:mCherry-Lc3)* line that marks autophagosomes, hereafter referred to as mCherry-Lc3. We found that GFP-2xFYVE and mCherry-Lc3 labelled autophagosomes rarely colocalise, but label distinct vesicles that occasionally are found in close proximity of each other (Figure S1C). Since the GFP-2xFYVE probe does not label autophagosomes, we therefore refer to vesicles labelled by GFP-2xFYVE in their membrane as 'early endosomes'.

Confocal imaging of the GFP-2xFYVE and mCherry-Dram1 transgenes in the accessible zebrafish tail fin tissue allowed us to study endosomal dynamics in great detail. Time-lapse imaging demonstrated

136 that globular mCherry-Dram1 labelled vesicles frequently interact with the PI(3)P-containing
137 membrane of early endosomes (Figure 1E). We could also observe mCherry-Dram1 vesicles forming
138 tethers between two distant early endosomes that are subsequently brought together (Figure 1E).
139 Ultimately, mCherry-Dram1 labelled vesicles fuse with early endosomes and localise to their lumen.
140 Early endosomes that have undergone such fusion events gradually lose the GFP-2xFYVE labelling of
141 their membrane, representing a reduction of PI(3)P lipids present in these membranes. Taken
142 together, ectopically expressed mCherry-Dram1 labels acidic and morphologically diverse vesicles that
143 interact and fuse with early endosomes. Subsequently, these early endosomes alter the PI lipid
144 composition of their membrane.

145 **Inhibiting PIKfyve and PI(3,5)P_2 formation affects mCherry-Dram1 labelled vesicles**

146 Early endosomes that have fused with mCherry-Dram1 labelled vesicles lose the GFP-2xFYVE labelling
147 of their membrane. We hypothesised that the enzymatic activity of the 1-phosphatidylinositol 3-
148 phosphate 5-kinase PIKfyve was responsible for the conversion of PI(3)P into PI(3,5)P_2 in this process.
149 To test this, we used YM201636 and apilimod to selectively inhibit the kinase activity of PIKfyve (Cai
150 et al., 2013; Jefferies et al., 2008). A block in PIKfyve activity is known to affect fusion and fission
151 events, which leads to membrane conservation and subsequent enlargement of endosomal
152 compartments (Choy et al., 2018; Ikonomov et al., 2003; Sbrissa et al., 1999). As expected, GFP-2xFYVE
153 zebrafish larvae treated with either YM201636 or apilimod displayed enlarged early endosomal
154 vesicles marked by PI(3)P in their membranes (Figure S2A). As the more potent and selective of the
155 two inhibitors (Cai et al., 2013), we tested a range of treatment durations for apilimod and found that
156 a relatively short incubation of 2 hours robustly enlarged GFP-2xFYVE labelled vesicles (Figure S2B).
157 We selected this treatment window for further experiments in which we exposed zebrafish larvae
158 expressing both the GFP-2xFYVE and mCherry-Dram1 constructs to either apilimod or DMSO as a
159 solvent control. We used confocal microscopy to image epithelial cells in the zebrafish tail fin and
160 analysed the number and morphology of GFP-2xFYVE and mCherry-Dram1 vesicles per cell (Figure S3).
161 Inhibition of the enzymatic activity of PIKfyve resulted in enlarged early endosomes and mCherry-
162 Dram1 labelled vesicles, while the number of both types of vesicles per cell was reduced (Figure 2A-
163 C). Furthermore, apilimod treatment significantly decreased the number of tubular mCherry-Dram1
164 vesicles per cell (Figure 2D & E). Therefore, mCherry-Dram1 labelled vesicles – that can interact and
165 fuse with early endosomes – are reduced in number and altered in their morphology when PIKfyve is
166 inhibited from converting PI(3)P on endosomal membranes into PI(3,5)P_2.

167 **mCherry-Dram1 accumulates in the lumen and on the membrane of early endosomes upon**
168 **inhibition of PI(3,5)P_2 formation**

169 Inhibiting PIKfyve to prevent the conversion of PI(3)P into PI(3,5)P_2 altered the number and
170 morphology of mCherry-Dram1 labelled vesicles, even though these vesicles themselves are initially
171 devoid of PI(3)P. This observation suggests that the conversion of PI(3)P into PI(3,5)P_2 on endosomal
172 membranes is important for the fate or function of mCherry-Dram1 labelled vesicles. Therefore, we
173 explored how inhibition of PIKfyve affects the localisation of mCherry-Dram1 and its interaction with
174 early endosomes containing PI(3)P in their membranes. Based on confocal images of GFP-2xFYVE and
175 mCherry-Dram1 in epithelial cells in the zebrafish tail fin, we could categorise mCherry-Dram1 signal
176 into four groups: 1) mCherry-Dram1 signal that is distant from early endosomes; 2) mCherry-Dram1
177 signal that is in close proximity or directly adjacent to early endosomes; 3) mCherry-Dram1 signal that
178 overlaps with the membrane of early endosomes; and 4) mCherry-Dram1 signal that is contained
179 within early endosomes (Figure 3A). We then used Fiji/ImageJ to analyse the localisation of mCherry-
180 Dram1 in respect to early endosomes according to these four categories (Figure S3). We found that
181 PIKfyve inhibition reduced the number of times mCherry-Dram1 was localised distant from, adjacent
182 to, or overlapping with early endosomal membranes, while it increased the number of times that

183 mCherry-Dram1 was contained within early endosomes (Figure 3B). However, since inhibition of
184 PIKfyve reduced the total number of mCherry-Dram1 vesicles per cell (Figure 2C), we also analysed
185 the categories as a percentage of the total mCherry-Dram1 labelled vesicles present in each cell. We
186 found that PIKfyve inhibition increased the percentage of mCherry-Dram1 signal that is contained
187 within early endosomes or overlaps with early endosomal membranes, at the expense of the
188 percentage of mCherry-Dram1 signal that is localised distant from or adjacent to early endosomes
189 (Figure 3C). In conclusion, mCherry-Dram1 accumulates in the lumen of early endosomes and on their
190 membranes when the conversion of PI(3)P into PI(3,5)P_2 is inhibited.

191 **Inhibition of PI(3,5)P_2 formation reduces the dynamic interactions between mCherry-Dram1 and**
192 **early endosomes**

193 The observation that mCherry-Dram1 labelled vesicles accumulated in and on early endosomes upon
194 inhibition of PIKfyve means that the dynamic interaction between these two types of vesicles was
195 altered. Either mCherry-Dram1 labelled vesicles interacted more frequently with early endosomes
196 upon inhibition of PIKfyve, or subsequent processes were inhibited that caused their accumulation.
197 We performed time-lapse imaging of the interactions between mCherry-Dram1 and early endosomes
198 to study these possible explanations. We exposed zebrafish larvae expressing both the GFP-2xFYVE
199 and mCherry-Dram1 constructs to either apilimod or DMSO as a solvent control and imaged epithelial
200 cells in the zebrafish tailfin after two hours of drug treatment using confocal microscopy (Figure 4A).
201 In the control group, we observed many interactions between mCherry-Dram1 and early endosomes
202 over time. This included temporary 'kiss-and-run' interactions, as well as long term contact between
203 two or more vesicles which frequently ended in mCherry-Dram1 fusing into early endosomes
204 (Supplementary movie 2). In contrast, inhibition of PIKfyve greatly reduced the motility of both types
205 of vesicles, with interactions taking place infrequently and novel fusion events between mCherry-
206 Dram1 and early endosomes only occurring rarely (Supplementary movie 3). Analysis of the number
207 of interactions that took place with mCherry-Dram1 per early endosome confirmed our observations,
208 as these were significantly reduced upon inhibition of PIKfyve (Figure 4B).
209
210 The anticipated effect of PIKfyve inhibition is that PI(3)P in the membrane of early endosomes can no
211 longer be converted into PI(3,5)P_2. As observed before (Figure 1E), early endosomes in the control
212 group gradually lost the PI(3)P lipids marked by GFP-2xFYVE in their membrane following fusion events
213 with mCherry-Dram1 (Figure 4A, Supplementary movie 2). Upon inhibition of PIKfyve, early
214 endosomes that had already fused with mCherry-Dram1, or underwent novel fusion events on rare
215 occasions, no longer lost the GFP-2xFYVE labelling of their membranes (Supplementary movie 3). By
216 quantifying this process for multiple time-lapse recordings, we confirmed that the duration for which
217 GFP-2xFYVE labelling of early endosomal membranes remained detectable following fusion with
218 mCherry-Dram1 vesicles was significantly increased upon PIKfyve inhibition (Figure 4C). Not all time-
219 lapse recordings of epithelial cells in zebrafish tail fins were of equal length due to technical difficulties
220 associated with this type of imaging in live animals (e.g. samples drifting out of focus). We therefore
221 also plotted the duration for which a GFP-2xFYVE ring containing mCherry-Dram1 signal remained
222 detectable in relation to the total duration for which the cell in which the fusion event occurred could
223 be followed (Figure 4D). This visualisation clearly illustrates the difference between the control group
224 in which mCherry-Dram1 frequently fused with early endosomes that subsequently lost the GFP-
225 2xFYVE labelling of their membrane, and the apilimod treated group in which the majority of early
226 endosomes containing mCherry-Dram1 signal retain the GFP-2xFYVE labelling of their membrane for
227 the entire duration of the time-lapse. Taken together, inhibition of PI(3,5)P_2 formation reduced the
228 dynamic interactions between mCherry-Dram1 and early endosomes, and caused mCherry-Dram1 to
229 accumulate in early endosomes by halting processes that normally follow upon vesicle fusion.

230
231 **Acidification of mCherry-Dram1 vesicles is reduced upon inhibition of PI(3,5)P_2 formation**
232 We have thus shown that early endosomes that have fused with mCherry-Dram1 labelled vesicles lose
233 the GFP-2xFYVE labelling of their membrane in a process dependent on the kinase activity of PIKfyve.
234 This loss of signal suggests that an endosomal maturation process takes place in which PI(3)P is
235 converted into PI(3,5)P_2 present in late endosomal membranes. The maturation of early into late
236 endosomes is associated with a decrease in luminal pH (Maxfield and Yamashiro, 1987). This prompted
237 us to investigate how inhibition of PIKfyve affected the acidification of early endosomes and mCherry-
238 Dram1 labelled vesicles. We therefore imaged GFP-2xFYVE and mCherry-Dram1 in epithelial cells in
239 the zebrafish tail fin, combined with LysoTracker staining to label acidic vesicles. In the control group,
240 we observed that the majority of mCherry-Dram1 labelled vesicles are acidic (Figure 5A), confirming
241 our earlier findings (Figure 1D and (van der Vaart et al., 2014)). GFP-2xFYVE labelled vesicles in the
242 control group varied in the extent of their acidity, ranging from (almost) no detectable LysoTracker
243 staining to clear staining of their lumen (Figure 5A). This variation in acidity for PI(3)P labelled vesicles
244 likely reflects the gradual acidification of early endosomes that takes place as they mature. Upon
245 inhibition of PIKfyve by apilimod treatment, early endosomes continue to display this range of luminal
246 acidification, with smaller PI(3)P labelled vesicles frequently not or dimly stained by LysoTracker and
247 larger vesicles typically stained intensely (Figure 5B). In contrast, mCherry-Dram1 labelled vesicles
248 appeared to be less frequently and less intensely stained by LysoTracker when PIKfyve was inhibited
249 (Figure 5B). We used Fiji/ImageJ to analyse the spatial overlap (colocalisation) between mCherry-
250 Dram1 and LysoTracker staining and found that the correlation between these two fluorescent signals
251 decreased significantly upon inhibition of PIKfyve (Figure 5C). We therefore conclude that the
252 acidification of mCherry-Dram1 vesicles is at least partially dependent on the formation of PI(3,5)P_2
253 by PIKfyve.
254
255 While analysing the colocalisation between mCherry-Dram1 and LysoTracker, we encountered
256 multiple large mCherry-Dram1 labelled vesicles that contained acidic (Lysotracker stained) and non-
257 acidic GFP-2xFYVE labelled vesicles (Figure 5D). These intraluminal vesicles appeared to accumulate
258 within the mCherry-Dram1 labelled compartments, forming what resembles a multivesicular body. To
259 visualise the dynamics of these events, we performed time-lapse imaging of GFP-2xFYVE and mCherry-
260 Dram1 combined with LysoTracker staining. In the control situation, a mCherry-Dram1$^+$/LysoTracker$^+$
261 vesicle formed a tether between two early endosomes with dim LysoTracker staining, causing the two
262 early endosomes to fuse together (Figure 5E and Supplementary movie 4). The mCherry-
263 Dram1$^+$/LysoTracker$^+$ vesicle continued to interact with this newly formed endosome and ultimately
264 fused with it. Following this fusion event, the early endosome displayed more intense luminal
265 LysoTracker staining and lost the GFP-2xFYVE labelling of its membrane over time. This maturation
266 process forms a stark contrast to what occurred upon inhibition of PIKfyve. As described before (Figure
267 4A), mCherry-Dram1 and GFP-2xFYVE labelled vesicles rarely interacted nor altered their existing
268 associations (Figure 5E and Supplementary movie 5). Large mCherry-Dram1 labelled vesicles varied in
269 their acidity, ranging from no or dim LysoTracker staining to intense LysoTracker staining. Inside the
270 lumen of non-acidified mCherry-Dram1 labelled compartments, we regularly observed small acidic
271 vesicles that moved around in a seemingly random pattern (Figure 5E and Supplementary movie 5).
272 These acidic intraluminal vesicles persisted over time, with no indication of releasing their content
273 into the lumen in which they reside. In conclusion, the kinase activity of PIKfyve is required for
274 mCherry-Dram1 labelled vesicles to tether early endosomes and fuse with them to kickstart a
275 maturation process in which their signature PI(3)P membrane lipids are converted and their lumen
276 further acidifies. When PIKfyve is inhibited, targeting of mCherry-Dram1 to acidic vesicles is reduced,

277 arresting mCherry-Dram1 in multivesicular bodies, early endosomes, or non-acidified vesicles halted
278 in their fusion with early endosomes.
279

280 Discussion

281 Degrading unwanted or harmful elements present in a cell or its microenvironment is important to
282 maintain cellular and tissue homeostasis. For instance, pathogenic protein aggregates can cause
283 diseases like Alzheimer's, Parkinson's, or Huntington's. Enhancing the delivery of pathogenic proteins
284 to the degradative environment of the lysosome is one possible therapeutic approach for these
285 protein aggregation diseases (Aguzzi and O'Connor, 2010). During microbial infection, degradation of
286 pathogens in lysosomes is a key immune defence function and enhancing the underlying vesicle
287 trafficking processes therefore presents a major opportunity for therapeutic strategies (Kaufmann et
288 al., 2018). For both examples, a thorough understanding of the molecular mechanisms controlling
289 endolysosomal and autophagic trafficking is required to successfully intervene in disease
290 pathogenesis. Here, we add to our understanding of these processes by studying the function of
291 Dram1 in vesicle trafficking in the optically transparent zebrafish model. We found that Dram1-
292 mediated vesicle fusion is dependent on the formation of PI(3,5)P_2 by PIKfyve to deliver vesicles and
293 their cargo to the acidic environment of endolysosomes.

294 The interplay between Dram1 and PIKfyve revealed by our study sheds light on the molecular
295 mechanisms underlying functions of Dram1 described in previous reports. Studies on mammalian cells
296 and in the zebrafish model found that DRAM1 (Dram1 in zebrafish) can induce autophagy and
297 stimulate vesicle fusion with lysosomes (Crighton et al., 2006; van der Vaart et al., 2014; Zhang et al.,
298 2013). This role of Dram1 is important in defence against mycobacterial infection in the zebrafish
299 model for tuberculosis, and mammalian DRAM1 was found to associate with *Mycobacterium*
300 *tuberculosis* phagocytosed by primary human macrophages (van der Vaart et al., 2014). Furthermore,
301 we recently described how zebrafish macrophages lacking Dram1 failed to deliver pathogenic
302 mycobacteria to acidic endolysosomal compartments, ultimately resulting in an inflammatory type of
303 cell death – called pyroptosis – which disseminates the infection (Zhang et al., 2020). Besides its
304 function in vesicle trafficking, DRAM1 is required for apoptosis mediated by the tumour suppressor
305 p53 in relation to cancer and in HIV infected CD4(+) T cells (Crighton et al., 2006; Laforge et al., 2013).
306 DRAM1 was shown to interact with the pro-apoptotic protein BAX, which recruited BAX to lysosomes
307 and initiated cell death via release of lysosomal cathepsin B (Guan et al., 2015). Recently, it has also
308 been found that DRAM1 is required for efficient activation of mTORC1, a nutrient-sensing complex
309 that functions at the lysosome (Beaumatin et al., 2019). DRAM1 facilitates activation of mTORC1 by
310 binding the membrane carrier protein SCAMP3 and the amino acid transporters SLC1A5 and LAT1,
311 thereby directing them to lysosomes (Beaumatin et al., 2019). An emerging theme is that DRAM1
312 functions at the interface between lysosomes, signalling complexes, and other vesicles by binding and
313 directing effector molecules. Our *in silico* analysis of predicted protein domains further supports a role
314 for DRAM1 as a protein binding hub important in the regulation of vesicle trafficking. Although Dram1-
315 mediated vesicle fusion and maturation events required the enzymatic activity of PIKfyve to generate
316 PI(3,5)P_2 on endosomal membranes, it remains unclear whether Dram1 directly interacted with these
317 molecules. Since the DRAM1 protein lacks consensus PI binding motifs (e.g. a FYVE domain), we expect
318 that effector proteins capable of binding either PI(3)P or PI(3,5)P_2 mediate this interaction.

319 The primary function of PIKfyve is to bind PI(3)P on endosomal membranes through its FYVE domain
320 and phosphorylate it into PI(3,5)P_2 (Shisheva, 2001). Besides this, PIKfyve can also phosphorylate PI to
321 generate PI(5)P, a low abundant PI family member found in different cellular compartments, including
322 the nucleus (Poli et al., 2019; Shisheva, 2001). PIKfyve functions as part of a complex scaffolded by

323 VAC14, also known as ArPIKfyve (Associated Regulator of PIKfyve) (Sbrissa et al., 2004). This complex
324 also contains Sac3, the phosphatase that converts PI(3,5)P_2 into PI(3)P (Sbrissa et al., 2008). The
325 presence of two enzymes with opposing activities in the same complex indicates that PI(3,5)P_2 levels
326 need to be tightly controlled. Indeed, inactivation of the PIKfyve containing complex impaired
327 autophagic and endolysosomal vesicle trafficking, thereby halting the maturation of these vesicles (de
328 Lartigue et al., 2009; Dong et al., 2010; Ferguson et al., 2009; Kim et al., 2014). The typical enlargement
329 of lysosomes upon inhibition of PIKfyve is ascribed to lysosome coalescence, most likely due to
330 reduced fission events during lysosomal 'kiss-and-run' interactions and/or full fusion and fission cycles
331 (Choy et al., 2018). Based on the data presented here, we propose that inhibition of PIKfyve prevents
332 DRAM1 from performing its function as an interface between lysosomes and vesicles destined for
333 fusion with lysosomes.

334 We took advantage of a fluorescently tagged version of zebrafish Dram1 to study its dynamic
335 localisation during vesicle trafficking events. This approach yielded valuable insights into the role of
336 DRAM1 in the endolysosomal maturation process, demonstrating that early endosomes labelled by
337 PI(3)P in their membrane mature and acidify following fusion events with mCherry-Dram1 labelled
338 vesicles. The overexpression of mCherry-Dram1 (driven by the zebrafish beta actin promoter) mimics
339 situations in which cells have upregulated the expression of DRAM1 in response to cellular stressors
340 like DNA damage or infection. However, this approach comes with a number of caveats regarding the
341 interpretation of our results, since ectopically expressed tagged proteins can exhibit altered behaviour
342 or expression patterns compared to their endogenous counterparts. For this reason, we place less
343 emphasis on the identity of mCherry-Dram1 labelled vesicles and rather focus on their activity and
344 interactions. Faithfull determination of the subcellular localisation of DRAM1 under different
345 circumstances would require an antibody staining approach to detect the endogenous protein, which
346 would preclude any dynamic observations. Furthermore, the expression of fluorescently tagged
347 proteins can alter cellular functions. It is known that expression of GFP-2xFYVE can alter endosomal
348 dynamics and induce sustained autophagosome formation (Nascimbeni et al., 2017). Therefore we
349 expect that GFP-2xFYVE interfered with PI(3)P interactions to some extent in our experiments, but the
350 strong effect of PIKfyve inhibition on endosomal dynamics indicates that most of the PI(3)P
351 functionality remains intact in the GFP-2xFYVE line. For mCherry-Dram1, we confirmed that the
352 relatively large fluorescent tag did not interfere with its known localisation to acidic vesicles, nor its
353 ability to induce autophagy upon overexpression. Nonetheless, a long sought-after goal in cell biology
354 remains to study endogenous protein dynamics in live cells without altering their functionality,
355 localisation, or expression level. Specifically for DRAM1, we aim to determine the function, identity,
356 and dynamics of globular and tubular vesicles containing endogenous DRAM1 in their membrane or
357 lumen.

358 Based on our observations, we conclude that mCherry-Dram labelled vesicles can tether early
359 endosomes and fuse with them as part of their maturation process. When we inhibited the formation
360 of PI(3,5)P_2 by PIKfyve, targeting of mCherry-Dram1 to acidic endolysosomal vesicles was reduced,
361 strongly suggesting that cargo carried by mCherry-Dram1 labelled vesicles is destined for degradation
362 in lysosomal compartments. In the zebrafish model for tuberculosis, we have previously demonstrated
363 that overexpression of Dram1 enhanced the localisation of mycobacteria to acidic endolysosomes (van
364 der Vaart et al., 2014). Further studies on the molecular mechanisms behind DRAM1-mediated vesicle
365 trafficking events will hopefully help to understand how it targets cargo to the degradative
366 environment of the lysosome. Such knowledge could form the basis for therapeutic approaches for a
367 spectrum of diseases in which unwanted elements reside inside a cell or in its microenvironment.

368

Material & methods

Zebrafish husbandry and care

Zebrafish lines in this study (listed in Supplementary table 1) were handled in compliance with local animal welfare regulations, as overseen by the Animal Welfare Body of Leiden University (License number: 10612) and maintained according to standard protocols (zfin.org). All experiments were performed on embryos or larvae up to 3 days post-fertilization (dpf), which have not yet reached the free-feeding stage. Embryos/larvae were kept in egg water (60 µg/ml Instant Ocean sea salts) at 28.5°C and treated with 0.02% ethyl 3-aminobenzoate methanesulfonate (Tricaine, Sigma-Aldrich) for anesthesia before imaging and fixation. For all experiments involving *Tg(bactin:mCherry-dram1)*, female adult zebrafish heterozygous for the transgene were outcrossed with male adult zebrafish of the required genotype (e.g. AB/TL wild type or carrying the GFP-x2FYVE transgenic construct). Offspring of these crosses were selected for proper expression of the transgenic constructs at 2 dpf by stereo fluorescent microscopy.

Generation of transgenic reporter lines

Full-length zebrafish Lc3 cDNA (*map1lc3b-201*; ENSDART00000163508.2) with attB sites added to its sequence was synthesised (BaseClear) and used to create a 3' Gateway entry vector (Invitrogen). This 3' Gateway entry vector was combined into a Tol2 containing destination vector together with a 5' Gateway entry vector containing the zebrafish beta actin promoter and a Gateway middle entry vector containing mCherry with the stop codon removed, generating the following DNA construct: *bactin:mCherry-Lc3*. For the generation of *Tg(bactin:mCherry-dram1)*, we used a DNA construct that was previously generated (van der Vaart et al., 2014). The DNA constructs were injected into AB/TL wildtype zebrafish embryos at the one cell stage (1 nl at 50 ng/µl), together with 50 pg Tol2 transposase mRNA to allow efficient integration into the genome. Zebrafish larvae were screened for appropriate expression of the constructs by stereo microscopy and reared into adulthood.

Drug treatment

Larvae were bath treated with apilimod (S6414, Selleck) or YM201636 (S1219, Selleck) diluted into egg water at a working concentration of 5 µM or 10 µM, respectively.

LysoTracker staining

Larvae were immersed in egg water containing 5 µM LysoTracker Deep Red (L12492, ThermoFisher) for 1 hour. Embryos were rinsed 3 times with egg water before imaging.

Confocal laser scanning microscopy

When appropriate, larvae were fixed in 4% formaldehyde (28906, ThermoFisher) in PBS solution overnight at 4°C. Fixed or Live embryos were mounted with 1.5% low melting agarose (140727, SERVA) in PBS or egg water, respectively. Basal cell layer epithelial cells were imaged in the thin and optically transparent tail fin area using a Leica TCS SP8 confocal microscope with a 63X oil immersion objective (NA = 1.4), and equipped with 488 nm, 532 nm, and 638 nm laser lines. For time-lapse imaging, confocal micrographs were acquired for a single focal plane at a time interval of ~1.3 second/image. Representative images were deconvoluted using the Iterative Deconvolution 3D plugin in Fiji/ImageJ (Dougherty, 2005).

Image analysis

Raw imaging data was analysed in Fiji/ImageJ to obtain measurements for vesicle morphology, interactions between vesicles, and colocalisation of fluorescent signals. For measurements of vesicle morphology, a maximum intensity Z-projection was generated for a single layer of epithelial cells imaged in the zebrafish tailfin tissue. Individual cells were selected and stored as regions of interest (ROIs) using the Polygon selection tool. The Phansalkar Auto-Local Threshold method was used for

414 segmentation of vesicles. Segmented vesicles that were directly adjacent to each other were separated
415 using a Watershed function. The resulting individual vesicles were measured per cell using the Analyze
416 Particles function.

417 To measure interactions between vesicles, the same method as described above was used to segment
418 individual vesicles per cell. Vesicles labelled by their respective fluorescent signal were stored as ROIs.
419 Subsequently, the distance between each mCherry-Dram1 ROI and the nearest GFP-2xFYVE labelled
420 ROI was determined. Based on this measurement, mCherry-Dram1 ROIs were categorised into four
421 groups: 1) mCherry-Dram1 ROI that is distant from a GFP-2xFYVE ROI (distance ≥ 5 pixels); 2) mCherry-
422 Dram1 ROI that is in close proximity or directly adjacent to a GFP-2xFYVE ROI (distance < 5 pixels); 3)
423 mCherry-Dram1 ROI that overlaps with a GFP-2xFYVE ROI; and 4) mCherry-Dram1 ROI that is
424 contained within a GFP-2xFYVE ROI. The Fiji/ImageJ plugin created to automate this analysis, called
425 'FYVE DRAM Analysis', is openly available for download via the Leiden University update site
426 (http://sites.imagej.net/Willemsejj/).

427 To analyse colocalisation between mCherry-Dram1 and LysoTracker Deep Red fluorescent signals, a
428 maximum intensity Z-projection was generated for a single layer of epithelial cells imaged in the
429 zebrafish tailfin tissue. The Gaussian Blur (sigma = 1) function was applied to decrease noise. After this,
430 the Li Threshold method, followed by the Analyze Particles function ('Show Mask'; size cut off of 10
431 pixels) was used to create a binary mask that excludes zero-zero pixels from the colocalisation analysis.
432 Finally, we used the Coloc 2 Fiji/ImageJ plugin (available via https://imagej.net/Coloc_2) to determine
433 the Pearson correlation coefficient between the two fluorescent signals.

434 **Statistical analysis and data representation**

435 Statistical analyses were performed using GraphPad Prism software (Version 5.01; GraphPad). All
436 experimental data (mean ± SEM) was analyzed using unpaired, two-tailed Mann–Whitney U tests for
437 comparisons between two groups and Kruskal–Wallis one-way analysis of variance with Dunn's
438 multiple comparison methods as a posthoc test for comparisons between more than two groups. (ns,
439 no significant difference; *p < 0.05; **p < 0.01; ***p < 0.001; ****p < 0.0001). The data sets from
440 each group are shown in a scatter plot (left) and a boxplot (right). In the scatter plots each dot
441 represents a data point, with the mean indicated by a horizontal line. Boxplots include 50% of the data
442 points, with a vertical line indicating the 95% confidence interval and a horizontal line indicating the
443 median. The only exception to this is Figure 2E, in which a violin plot is shown to represent the spread
444 of individual data points due to the large number of 0 values which would distort the scatter plot.

445 Acknowledgements

446 We thank Monica Varela and Rubén Marín Juez for critical proof reading of the manuscript. We are
447 grateful to all members of the fish facility team for zebrafish care. M.v.d.V. was supported by the
448 Netherlands Technology Foundation TTW (project 13259). S.M.S. was funded by the European Union's
449 Horizon 2020 research and innovation programme under the Marie Sklodowska-Curie grant
450 agreement No. 721537. G.F.-C. was funded by a European Marie Curie fellowship (H2020-COFUND-
451 2015-FP707404).

452 References

453 Aguzzi, A., O'Connor, T., 2010. Protein aggregation diseases: pathogenicity and therapeutic
454 perspectives. Nat. Rev. Drug Discov. 9, 237–248. https://doi.org/10.1038/nrd3050
455 Banerjee, S., Kane, P.M., 2020. Regulation of V-ATPase Activity and Organelle pH by
456 Phosphatidylinositol Phosphate Lipids. Front. Cell Dev. Biol. 8.
457 https://doi.org/10.3389/fcell.2020.00510
458 Beaumatin, F., O'Prey, J., Barthet, V.J.A., Zunino, B., Parvy, J.-P., Bachmann, A.M., O'Prey, M., Kania,
459 E., Gonzalez, P.S., Macintosh, R., Lao, L.Y., Nixon, C., Lopez, J., Long, J.S., Tait, S.W.G., Ryan,
460 K.M., 2019. mTORC1 Activation Requires DRAM-1 by Facilitating Lysosomal Amino Acid
461 Efflux. Mol. Cell 76, 163-176.e8. https://doi.org/10.1016/j.molcel.2019.07.021
462 Cai, X., Xu, Y., Cheung, A.K., Tomlinson, R.C., Alcázar-Román, A., Murphy, L., Billich, A., Zhang, B.,
463 Feng, Y., Klumpp, M., Rondeau, J.-M., Fazal, A.N., Wilson, C.J., Myer, V., Joberty, G.,
464 Bouwmeester, T., Labow, M.A., Finan, P.M., Porter, J.A., Ploegh, H.L., Baird, D., De Camilli, P.,
465 Tallarico, J.A., Huang, Q., 2013. PIKfyve, a class III PI kinase, is the target of the small
466 molecular IL-12/IL-23 inhibitor apilimod and a player in Toll-like receptor signaling. Chem.
467 Biol. 20, 912–921. https://doi.org/10.1016/j.chembiol.2013.05.010
468 Choy, C.H., Saffi, G., Gray, M.A., Wallace, C., Dayam, R.M., Ou, Z.-Y.A., Lenk, G., Puertollano, R.,
469 Watkins, S.C., Botelho, R.J., 2018. Lysosome enlargement during inhibition of the lipid kinase
470 PIKfyve proceeds through lysosome coalescence. J. Cell Sci. 131.
471 https://doi.org/10.1242/jcs.213587
472 Cossart, P., Helenius, A., 2014. Endocytosis of Viruses and Bacteria. Cold Spring Harb. Perspect. Biol.
473 6. https://doi.org/10.1101/cshperspect.a016972
474 Crighton, D., Wilkinson, S., O'Prey, J., Syed, N., Smith, P., Harrison, P.R., Gasco, M., Garrone, O.,
475 Crook, T., Ryan, K.M., 2006. DRAM, a p53-induced modulator of autophagy, is critical for
476 apoptosis. Cell 126, 121–134. https://doi.org/10.1016/j.cell.2006.05.034
477 de Lartigue, J., Polson, H., Feldman, M., Shokat, K., Tooze, S.A., Urbé, S., Clague, M.J., 2009. PIKfyve
478 regulation of endosome-linked pathways. Traffic Cph. Den. 10, 883–893.
479 https://doi.org/10.1111/j.1600-0854.2009.00915.x
480 Deretic, V., Saitoh, T., Akira, S., 2013. Autophagy in infection, inflammation and immunity. Nat. Rev.
481 Immunol. 13, 722–737. https://doi.org/10.1038/nri3532
482 Dong, X., Shen, D., Wang, X., Dawson, T., Li, X., Zhang, Q., Cheng, X., Zhang, Y., Weisman, L.S.,
483 Delling, M., Xu, H., 2010. PI(3,5)P(2) controls membrane trafficking by direct activation of
484 mucolipin Ca(2+) release channels in the endolysosome. Nat. Commun. 1, 38.
485 https://doi.org/10.1038/ncomms1037
486 Dougherty, R., 2005. Extensions of DAMAS and Benefits and Limitations of Deconvolution in
487 Beamforming, in: 11th AIAA/CEAS Aeroacoustics Conference, Aeroacoustics Conferences.
488 American Institute of Aeronautics and Astronautics. https://doi.org/10.2514/6.2005-2961
489 Fader, C.M., Colombo, M.I., 2009. Autophagy and multivesicular bodies: two closely related partners.
490 Cell Death Differ. 16, 70–78. https://doi.org/10.1038/cdd.2008.168
491 Ferguson, C.J., Lenk, G.M., Meisler, M.H., 2009. Defective autophagy in neurons and astrocytes from
492 mice deficient in PI(3,5)P2. Hum. Mol. Genet. 18, 4868–4878.
493 https://doi.org/10.1093/hmg/ddp460
494 Futter, C.E., Collinson, L.M., Backer, J.M., Hopkins, C.R., 2001. Human VPS34 is required for internal
495 vesicle formation within multivesicular endosomes. J. Cell Biol. 155, 1251–1264.
496 https://doi.org/10.1083/jcb.200108152
497 Glick, D., Barth, S., Macleod, K.F., 2010. Autophagy: cellular and molecular mechanisms. J. Pathol.
498 221, 3–12. https://doi.org/10.1002/path.2697
499 Guan, J.-J., Zhang, X.-D., Sun, W., Qi, L., Wu, J.-C., Qin, Z.-H., 2015. DRAM1 regulates apoptosis
500 through increasing protein levels and lysosomal localization of BAX. Cell Death Dis. 6, e1624–
501 e1624. https://doi.org/10.1038/cddis.2014.546

502 Hammond, G.R.V., Fischer, M.J., Anderson, K.E., Holdich, J., Koteci, A., Balla, T., Irvine, R.F., 2012.
503 PI4P and PI(4,5)P2 are essential but independent lipid determinants of membrane identity.
504 Science 337, 727–730. https://doi.org/10.1126/science.1222483
505 He, C., Bartholomew, C.R., Zhou, W., Klionsky, D.J., 2009. Assaying autophagic activity in transgenic
506 GFP-Lc3 and GFP-Gabarap zebrafish embryos. Autophagy 5, 520–526.
507 https://doi.org/10.4161/auto.5.4.7768
508 Heo, W.D., Inoue, T., Park, W.S., Kim, M.L., Park, B.O., Wandless, T.J., Meyer, T., 2006. PI(3,4,5)P3
509 and PI(4,5)P2 lipids target proteins with polybasic clusters to the plasma membrane. Science
510 314, 1458–1461. https://doi.org/10.1126/science.1134389
511 Huotari, J., Helenius, A., 2011. Endosome maturation. EMBO J. 30, 3481–3500.
512 https://doi.org/10.1038/emboj.2011.286
513 Ikonomov, O.C., Sbrissa, D., Foti, M., Carpentier, J.-L., Shisheva, A., 2003. PIKfyve Controls Fluid
514 Phase Endocytosis but Not Recycling/Degradation of Endocytosed Receptors or Sorting of
515 Procathepsin D by Regulating Multivesicular Body Morphogenesis. Mol. Biol. Cell 14, 4581–
516 4591. https://doi.org/10.1091/mbc.E03-04-0222
517 Jefferies, H.B.J., Cooke, F.T., Jat, P., Boucheron, C., Koizumi, T., Hayakawa, M., Kaizawa, H., Ohishi, T.,
518 Workman, P., Waterfield, M.D., Parker, P.J., 2008. A selective PIKfyve inhibitor blocks
519 PtdIns(3,5)P(2) production and disrupts endomembrane transport and retroviral budding.
520 EMBO Rep. 9, 164–170. https://doi.org/10.1038/sj.embor.7401155
521 Kaufmann, S.H.E., Dorhoi, A., Hotchkiss, R.S., Bartenschlager, R., 2018. Host-directed therapies for
522 bacterial and viral infections. Nat. Rev. Drug Discov. 17, 35–56.
523 https://doi.org/10.1038/nrd.2017.162
524 Kim, G.H.E., Dayam, R.M., Prashar, A., Terebiznik, M., Botelho, R.J., 2014. PIKfyve inhibition
525 interferes with phagosome and endosome maturation in macrophages. Traffic Cph. Den. 15,
526 1143–1163. https://doi.org/10.1111/tra.12199
527 Kumar, M., Gouw, M., Michael, S., Sámano-Sánchez, H., Pancsa, R., Glavina, J., Diakogianni, A.,
528 Valverde, J.A., Bukirova, D., Čalyševa, J., Palopoli, N., Davey, N.E., Chemes, L.B., Gibson, T.J.,
529 2020. ELM-the eukaryotic linear motif resource in 2020. Nucleic Acids Res. 48, D296–D306.
530 https://doi.org/10.1093/nar/gkz1030
531 Laforge, M., Limou, S., Harper, F., Casartelli, N., Rodrigues, V., Silvestre, R., Haloui, H., Zagury, J.-F.,
532 Senik, A., Estaquier, J., 2013. DRAM triggers lysosomal membrane permeabilization and cell
533 death in CD4(+) T cells infected with HIV. PLoS Pathog. 9, e1003328.
534 https://doi.org/10.1371/journal.ppat.1003328
535 Mah, L.Y., O'Prey, J., Baudot, A.D., Hoekstra, A., Ryan, K.M., 2012. DRAM-1 encodes multiple
536 isoforms that regulate autophagy. Autophagy 8, 18–28.
537 https://doi.org/10.4161/auto.8.1.18077
538 Malik, B.R., Maddison, D.C., Smith, G.A., Peters, O.M., 2019. Autophagic and endo-lysosomal
539 dysfunction in neurodegenerative disease. Mol. Brain 12, 100.
540 https://doi.org/10.1186/s13041-019-0504-x
541 Maxfield, F.R., Yamashiro, D.J., 1987. Endosome acidification and the pathways of receptor-
542 mediated endocytosis. Adv. Exp. Med. Biol. 225, 189–198. https://doi.org/10.1007/978-1-
543 4684-5442-0_16
544 Nascimbeni, A.C., Codogno, P., Morel, E., 2017. Local detection of PtdIns3P at autophagosome
545 biogenesis membrane platforms. Autophagy 13, 1602–1612.
546 https://doi.org/10.1080/15548627.2017.1341465
547 Naslavsky, N., Caplan, S., 2005. C-terminal EH-domain-containing proteins: consensus for a role in
548 endocytic trafficking, EH? J. Cell Sci. 118, 4093–4101. https://doi.org/10.1242/jcs.02595
549 Odorizzi, G., Babst, M., Emr, S.D., 1998. Fab1p PtdIns(3)P 5-kinase function essential for protein
550 sorting in the multivesicular body. Cell 95, 847–858. https://doi.org/10.1016/s0092-
551 8674(00)81707-9

552 Poli, A., Zaurito, A.E., Abdul-Hamid, S., Fiume, R., Faenza, I., Divecha, N., 2019. Phosphatidylinositol 5
553 Phosphate (PI5P): From Behind the Scenes to the Front (Nuclear) Stage. Int. J. Mol. Sci. 20.
554 https://doi.org/10.3390/ijms20092080
555 Raiborg, C., Bache, K.G., Gillooly, D.J., Madshus, I.H., Stang, E., Stenmark, H., 2002. Hrs sorts
556 ubiquitinated proteins into clathrin-coated microdomains of early endosomes. Nat. Cell Biol.
557 4, 394–398. https://doi.org/10.1038/ncb791
558 Rasmussen, J.P., Sack, G.S., Martin, S.M., Sagasti, A., 2015. Vertebrate Epidermal Cells Are Broad-
559 Specificity Phagocytes That Clear Sensory Axon Debris. J. Neurosci. 35, 559–570.
560 https://doi.org/10.1523/JNEUROSCI.3613-14.2015
561 Sachse, M., Urbé, S., Oorschot, V., Strous, G.J., Klumperman, J., 2002. Bilayered clathrin coats on
562 endosomal vacuoles are involved in protein sorting toward lysosomes. Mol. Biol. Cell 13,
563 1313–1328. https://doi.org/10.1091/mbc.01-10-0525
564 Saha, S., Panigrahi, D.P., Patil, S., Bhutia, S.K., 2018. Autophagy in health and disease: A
565 comprehensive review. Biomed. Pharmacother. 104, 485–495.
566 https://doi.org/10.1016/j.biopha.2018.05.007
567 Sbrissa, D., Ikonomov, O.C., Fenner, H., Shisheva, A., 2008. ArPIKfyve Homomeric and Heteromeric
568 Interactions Scaffold PIKfyve and Sac3 in a Complex to Promote PIKfyve Activity and
569 Functionality. J. Mol. Biol. 384, 766–779. https://doi.org/10.1016/j.jmb.2008.10.009
570 Sbrissa, D., Ikonomov, O.C., Shisheva, A., 1999. PIKfyve, a mammalian ortholog of yeast Fab1p lipid
571 kinase, synthesizes 5-phosphoinositides. Effect of insulin. J. Biol. Chem. 274, 21589–21597.
572 https://doi.org/10.1074/jbc.274.31.21589
573 Sbrissa, D., Ikonomov, O.C., Strakova, J., Dondapati, R., Mlak, K., Deeb, R., Silver, R., Shisheva, A.,
574 2004. A Mammalian Ortholog of Saccharomyces cerevisiae Vac14 That Associates with and
575 Up-Regulates PIKfyve Phosphoinositide 5-Kinase Activity. Mol. Cell. Biol. 24, 10437–10447.
576 https://doi.org/10.1128/MCB.24.23.10437-10447.2004
577 Shisheva, A., 2001. PIKfyve: the road to PtdIns 5-P and PtdIns 3,5-P(2). Cell Biol. Int. 25, 1201–1206.
578 https://doi.org/10.1006/cbir.2001.0803
579 Strahl, T., Thorner, J., 2007. Synthesis and Function of Membrane Phosphoinositides in Budding
580 Yeast, Saccharomyces cerevisiae. Biochim. Biophys. Acta 1771, 353–404.
581 https://doi.org/10.1016/j.bbalip.2007.01.015
582 Sun, A., 2018. Lysosomal storage disease overview. Ann. Transl. Med. 6.
583 https://doi.org/10.21037/atm.2018.11.39
584 Tzeng, H.-T., Wang, Y.-C., 2016. Rab-mediated vesicle trafficking in cancer. J. Biomed. Sci. 23.
585 https://doi.org/10.1186/s12929-016-0287-7
586 van der Vaart, M., Korbee, C.J., Lamers, G.E.M., Tengeler, A.C., Hosseini, R., Haks, M.C., Ottenhoff,
587 T.H.M., Spaink, H.P., Meijer, A.H., 2014. The DNA damage-regulated autophagy modulator
588 DRAM1 links mycobacterial recognition via TLR-MYD88 to autophagic defense [corrected].
589 Cell Host Microbe 15, 753–767. https://doi.org/10.1016/j.chom.2014.05.005
590 Wallroth, A., Haucke, V., 2018. Phosphoinositide conversion in endocytosis and the endolysosomal
591 system. J. Biol. Chem. 293, 1526–1535. https://doi.org/10.1074/jbc.R117.000629
592 Zerial, M., McBride, H., 2001. Rab proteins as membrane organizers. Nat. Rev. Mol. Cell Biol. 2, 107–
593 117. https://doi.org/10.1038/35052055
594 Zhang, R., Varela, M., Forn-Cuní, G., Torraca, V., van der Vaart, M., Meijer, A.H., 2020. Deficiency in
595 the autophagy modulator Dram1 exacerbates pyroptotic cell death of Mycobacteria-infected
596 macrophages. Cell Death Dis. 11, 1–16. https://doi.org/10.1038/s41419-020-2477-1
597 Zhang, X.-D., Qi, L., Wu, J.-C., Qin, Z.-H., 2013. DRAM1 regulates autophagy flux through lysosomes.
598 PloS One 8, e63245. https://doi.org/10.1371/journal.pone.0063245
599

600 Figure legends

601 **Figure 1: Transmembrane protein Dram1 mainly localises to acidic vesicles and interacts with early**
602 **endosomes.** (A) Schematic representation of protein domains predicted by the Eukaryotic Linear
603 Motif (ELM) resource in the human DRAM1 protein (UniProtKB: Q8N682). (B) Schematic
604 representation of the region of interest (ROI) used for confocal imaging of basal cell layer epithelial
605 cells in the tailfin of 3 days post fertilisation (dpf) zebrafish larvae. (C) Representative stills from time-
606 lapse confocal imaging of mCherry-Dram1. A globular mCherry-Dram1 labelled vesicle displaying a
607 tubular extension is indicated by an asterix (*). A motile tubular mCherry-Dram1 labelled vesicle is
608 indicated by arrowheads (Δ). The intensity calibration bar for the Lookup table (LUT) is displayed in
609 the top panel, ranging from 0 to 255. (D) Representative maximum intensity Z-projection of basal cell
610 layer epithelial cells expressing mCherry-Dram1 and stained with LysoTracker Deep Red. Panels (from
611 left to right) display the merged image, mCherry-Dram1 in magenta, and LysoTracker Deep red in
612 yellow. (E) Representative stills from time-lapse confocal imaging of mCherry-Dram1 and GFP-2xFYVE
613 in basal cell layer epithelial cells. The top panels display the merged image for each time point with
614 mCherry-Dram1 in magenta and GFP-2xFYVE in cyan, while the panels below show GFP-2xFYVE and
615 mCherry-Dram1 seperately. A tether formed by mCherry-Dram1 between two GFP-2xFYVE labelled
616 vesicles is indicated by an asterisk (*). The arrowheads (Δ) indicate a GFP-2xFYVE labelled vesicle that
617 fuses with mCherry-Dram1 (t=0s and t=20s) and subsequently loses the GFP-2xFYVE labelling of its
618 membrane (t=135s and t=155s). Scale bars: 5 µm.

619 **Figure 2: Inhibiting the formation of PI(3,5)P_2 affects the morphology and number of mCherry-**
620 **Dram1 labelled vesicles.** Zebrafish larvae (3 dpf) expressing mCherry-Dram1 and GFP-2xFYVE were
621 treated for 2 hours with 5 µm apilimod or DMSO as a solvent control. (A) Representative maximum
622 intensity Z-projection of mCherry-Dram1 and GFP-2xFYVE in basal cell layer epithelial cells. The left
623 hand panels display the merged image with mCherry-Dram1 in magenta and GFP-2xFYVE in cyan,
624 while the right hand panels show only mCherry-Dram1. (B) Quantification of the average size of GFP-
625 2xFYVE (FYVE) and mCherry-Dram1 (Dram1) labelled vesicles per basal cell layer epithelial cell. (C)
626 Quantification of the number of GFP-2xFYVE (FYVE) and mCherry-Dram1 (Dram1) labelled vesicles per
627 basal cell layer epithelial cell. (D) Maximum intensity Z-projection of mCherry-Dram1 and GFP-2xFYVE
628 in basal cell layer epithelial cells displaying multiple tubular mCherry-Dram1 labelled vesicles
629 (indicated by asterisks, *). (E) Quantification of the number of tubular mCherry-Dram1 labelled
630 vesicles per basal cell layer epithelial cell. Tubular vesicles are defined as vesicles with a length that is
631 at least two times longer than their width. Quantifications (B, C, E) were performed on n = 160 cells
632 for the DMSO group and n = 173 cells for the apilimod treated group. For both conditions, these cells
633 were imaged in the tailfins of 17 zebrafish larvae derived from 2 independent experiments. Scale bars:
634 5 µm.

635 **Figure 3: Dram1 accumulates in early endosomes and on early endosomal membranes upon**
636 **inhibition of PI(3,5)P_2 formation.** Zebrafish larvae (3 dpf) expressing mCherry-Dram1 and GFP-2xFYVE
637 were treated for 2 hours with 5 µm apilimod or DMSO as a solvent control. (A) Maximum intensity Z-
638 projection of mCherry-Dram1 and GFP-2xFYVE in basal cell layer epithelial cells illustrating the 4 types
639 of interactions that were categorised. Top panels: DMSO treated controls. Bottom panels: apilimod
640 treated. Boxed areas in the merged images on the left hand side (numbered 1 to 4) are detailed on
641 the right hand side, with mCherry-Dram1 in magenta and GFP-2xFYVE in cyan. (B) Quantification of
642 the 4 types of interactions between mCherry-Dram1 and GFP-2xFYVE labelled vesicles per basal cell
643 layer epithelial cell. (C) Quantification of the 4 types of interaction between mCherry-Dram1 and GFP-
644 2xFYVE labelled vesicles per basal cell layer epithelial cell, displayed as percentage of the total number
645 of mCherry-Dram1 labelled vesicles in a cell. Quantifications were performed on n = 160 cells for the

646 DMSO group and n = 173 cells for the apilimod treated group. For both conditions, these cells were
647 imaged in the tailfins of 17 zebrafish larvae derived from 2 independent experiments. Scale bars: 5
648 µm.

649

650 **Figure 4: Interaction and fusion between Dram1-containing vesicles and early endosomes is reduced**
651 **upon inhibition of PI(3,5)P_2 formation.** Zebrafish larvae (3 dpf) expressing mCherry-Dram1 and GFP-
652 2xFYVE were treated for 2 hours with 5 µm apilimod or DMSO as a solvent control. (A) Representative
653 stills from time-lapse confocal imaging of mCherry-Dram1 and GFP-2xFYVE in basal cell layer epithelial
654 cells. The top panels display the merged image for each time point with mCherry-Dram1 in magenta
655 and GFP-2xFYVE in cyan, while the bottom panels show only mCherry-Dram1. The arrowheads (Δ)
656 indicate a GFP-2xFYVE labelled vesicle that fuses with mCherry-Dram1 (t=90s and t=190s) and
657 subsequently loses the GFP-2xFYVE labelling of its membrane (t=580s). (B) Quantification of the
658 number of observed interactions between mCherry-Dram1 and GFP-2xFYVE labelled vesicles per
659 minute. For the DMSO control group, the interactions of n = 248 GFP-2xFYVE labelled vesicles with
660 mCherry-Dram1 imaged in 29 different cells were quantified for the duration of the time lapses. For
661 the apilimod treated group, the interactions of n = 341 GFP-2xFYVE labelled vesicles with mCherry-
662 Dram1 imaged in 40 different cells were quantified for the duration of the time lapses. (C)
663 Quantification of the duration for which GFP-2xFYVE labelling of membranes could be observed
664 following fusion with mCherry-Dram1 labelled vesicles (DMSO: n = 45 fusion events in 29 cells;
665 apilimod: n = 26 fusion events in 40 cells). (D) Visualisation of the duration for which GFP-2xFYVE
666 labelling of membranes could be observed following fusion with mCherry-Dram1 labelled vesicles,
667 relative to the length of time for which the vesicle could be imaged. Horizontal light-grey bars indicate
668 the length of time for which the cell could be imaged. A yellow (DMSO) or blue (apilimod) horizontal
669 bar indicates the moment of fusion, up until the moment the GFP-2xFYVE labelling of the membrane
670 could no longer be observed. Scale bars: 5 µm.

671 **Figure 5: Acidification of Dram1-containing vesicles is reduced upon inhibition of PI(3,5)P_2**
672 **formation, arresting Dram1 in early endosomes and MVBs.** Zebrafish larvae (3 dpf) expressing
673 mCherry-Dram1 and GFP-2xFYVE and stained with LysoTracker Deep Red were treated for 2 hours
674 with 5 µm apilimod or DMSO as a solvent control. (A, B) Representative maximum intensity Z-
675 projection of mCherry-Dram1, GFP-2xFYVE, and LysoTracker Deep Red in basal cell layer epithelial
676 cells. The left hand panels display the merged image with mCherry-Dram1 in magenta, GFP-2xFYVE in
677 cyan, and LysoTracker in yellow, while the middle and right hand panels show only mCherry-Dram1
678 and LysoTracker, respectively. The boxed area in the DMSO panels indicates GFP-2xFYVE labelled
679 vesicles with LysoTracker staining ranging from dim to intense. The boxed area in the apilimod panels
680 indicates mCherry-Dram1 labelled vesicles with LysoTracker staining ranging from dim to intense. (C)
681 The Pearson's R value correlation between mCherry-Dram1 and LysoTracker Deep Red fluorescent
682 signal was determined for confocal images of basal cell layer epithelial cells in the tailfin of n = 18
683 (DMSO) and n = 14 (apilimod) zebrafish larvae derived from two independent experiments. Each of
684 these images contained multiple epithelial cells. (D) Maximum intensity Z-projection of mCherry-
685 Dram1, GFP-2xFYVE, and LysoTracker Deep Red in a basal cell layer epithelial cell treated with
686 apilimod. The encircled area indicates a mCherry-Dram1 labelled compartment containing (remnants
687 of) other vesicles positive for either GFP-2xFYVE or LysoTracker Deep Red. (E) Representative stills
688 from time-lapse confocal imaging of mCherry-Dram1, GFP-2xFYVE, and LysoTracker Deep Red in basal
689 cell layer epithelial cells. The top panels display the merged image for each time point with mCherry-
690 Dram1 in magenta, GFP-2xFYVE in cyan, and LysoTracker Deep Red in yellow. The middle and bottom
691 panels show only mCherry-Dram1, or LysoTracker Deep Red respectively. A tether formed by mCherry-

692 Dram1 between two GFP-2xFYVE labelled vesicles is indicated by an asterix (*). The arrowheads (Δ) in
693 DMSO panels indicate a GFP-2xFYVE labelled vesicle that fuses with mCherry-Dram1 (t=65s and
694 t=115s) and subsequently loses the GFP-2xFYVE labelling of its membrane while increasing the
695 intensity of its LysoTracker Deep Red staining (t=180s). The arrowheads (Δ) in apilimod panels indicate
696 a LysoTracker Deep Red stained intraluminal vesicle moving inside a mCherry-Dram1 labelled
697 compartment. Scale bars: 5 µm (A, B and D) or 2 µm (E).

698 **Supplementary figure 1**, supporting Figure 1: Representative maximum intensity Z-projections of
699 basal cell layer epithelial cells imaged in the tailfin of 3 days post fertilisation (dpf) zebrafish larvae.
700 (A) Epithelial cells expressing mCherry-Dram1 and GFP-Lc3. Panels (from left to right) display the
701 merged image, mCherry-Dram1 in magenta, and GFP-Lc3 in green. (B) Same as described for (A), with
702 the exception that the offspring of heterozygous *Tg(bactin:mCherry-dram1)* animals outcrossed with
703 *Tg(CMV:GFP-Lc3)* animals was sorted into groups that were either positive or negative for the
704 mCherry-Dram1 construct, while all expressed the GFP-Lc3 construct. Top panels: expressing the
705 mCherry-Dram1 construct (+ mCherry-Dram1). Bottom panels: not expressing the mCherry-Dram1
706 construct (- mCherry-Dram1). (C) Epithelial cells expressing mCherry-Lc3 and GFP-2xFYVE. Panels
707 (from left to right) display the merged image, GFP-2xFYVE in cyan and mCherry-Lc3 in magenta. Scale
708 bars: 5 µm.

709 **Supplementary figure 2**, supporting Figure 2: (A) Zebrafish larvae (3 dpf) expressing GFP-2xFYVE were
710 treated for 2 hours with 5 µm apilimod, 10 µm YM201636, or DMSO as a solvent control.
711 Representative maximum intensity Z-projection of GFP-2xFYVE in basal cell layer epithelial cells. (B)
712 Zebrafish larvae (3 dpf) expressing GFP-2xFYVE were treated for 1, 2, 3, or 24 hours prior to fixation
713 and imaging with 5 µm apilimod or DMSO as a solvent control. The average area of GFP-2xFYVE
714 labelled vesicles per cell was measured using Fiji/ImageJ. N ≥ 7 individual zebrafish larvae per group.

715 **Supplementary figure 3**, supporting Figure 2: (A) Representative maximum intensity Z-projection of
716 basal cell layer epithelial cells expressing mCherry-Dram1 and GFP-2xFYVE, imaged in the tailfin of a 3
717 days post fertilisation (dpf) zebrafish larvae. (B) Example of a manually segmented epithelial cell based
718 on a high-intensity representation of GFP-2xFYVE signal present in the cell. (C) Example of vesicle
719 segmentation as performed by Fiji/Image.

720

721 **Supplementary table 1: Zebrafish lines used in this study**

Line	Description	Reference
AB/TL	Wild type strain	-
TgBAC (ΔNp63:Gal4FF)^{la213}	Gal4 driver line specific for basal cell layer epithelial cells	(Rasmussen et al., 2015)
Tg(4xUAS:EGFP-2xFYVE)^{la214}	Fluorescent probe labelling PI(3)P membrane lipids	(Rasmussen et al., 2015)
Tg(CMV:GFP-Lc3)	GFP-tagged zebrafish Lc3	(He et al., 2009)
Tg(bactin:mCherry-Lc3)	mCherry-tagged zebrafish Lc3	This study
Tg(bactin:mCherry-dram1)	mCherry-tagged zebrafish Dram1	This study

722

723

724

<Figure 1>

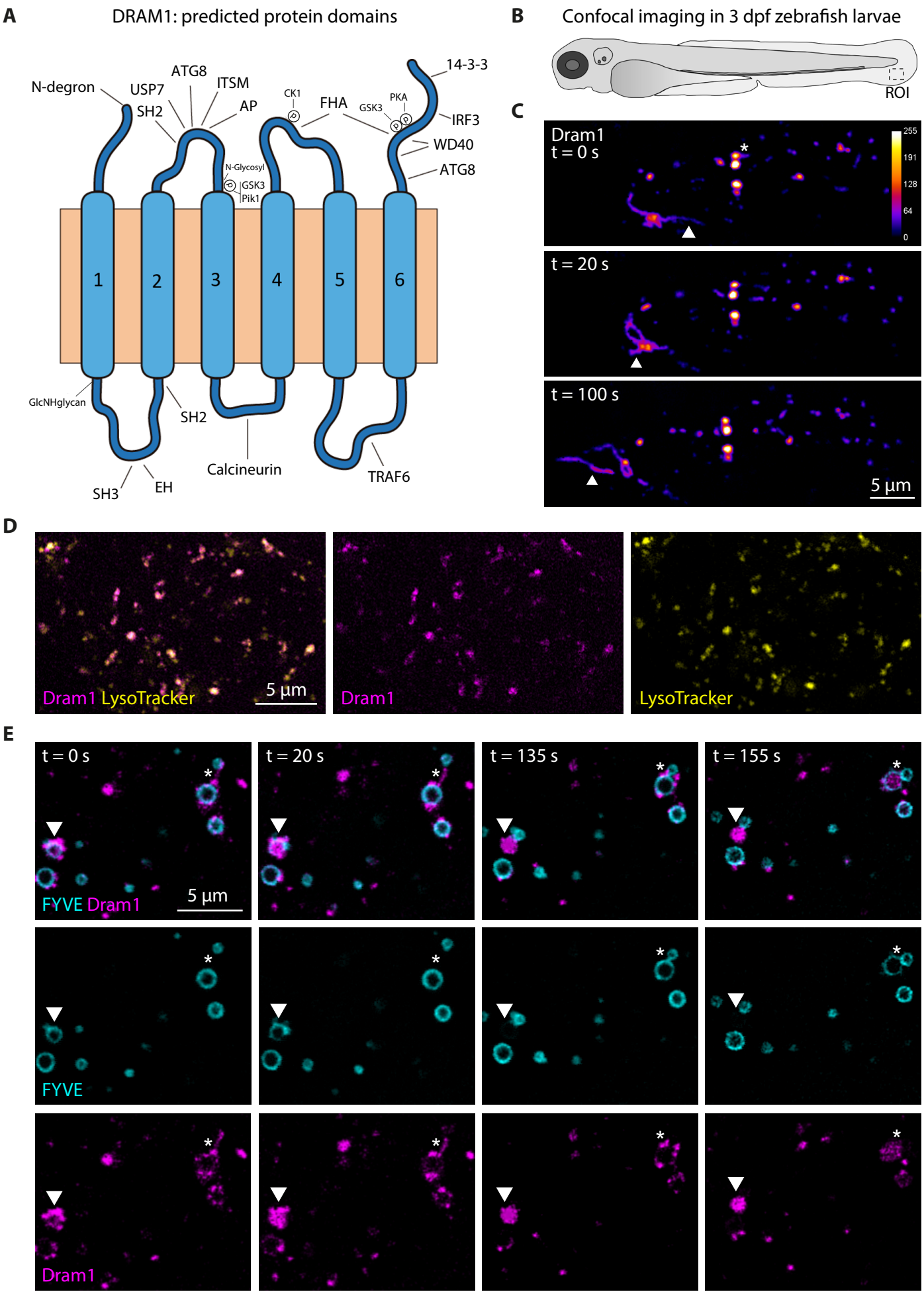
A
DRAM1: predicted protein domains
N-degron
USP7
SH2
ATG8
ITSM
AP
CK1
FHA
GSK3
PKA
14-3-3
IRF3
WD40
ATG8
N-Glycosyl
GSK3
Pik1
1
2
3
4
5
6
GlcNHglycan
SH2
Calcineurin
TRAF6
SH3
EH
B
Confocal imaging in 3 dpf zebrafish larvae
ROI
C
Dram1
t = 0 s
255
191
128
64
0
t = 20 s
t = 100 s
5 µm
D
Dram1 LysoTracker
5 µm
Dram1
LysoTracker
E
t = 0 s
t = 20 s
t = 135 s
t = 155 s
FYVE Dram1
5 µm
FYVE
Dram1

<Supplementary Figure 1>

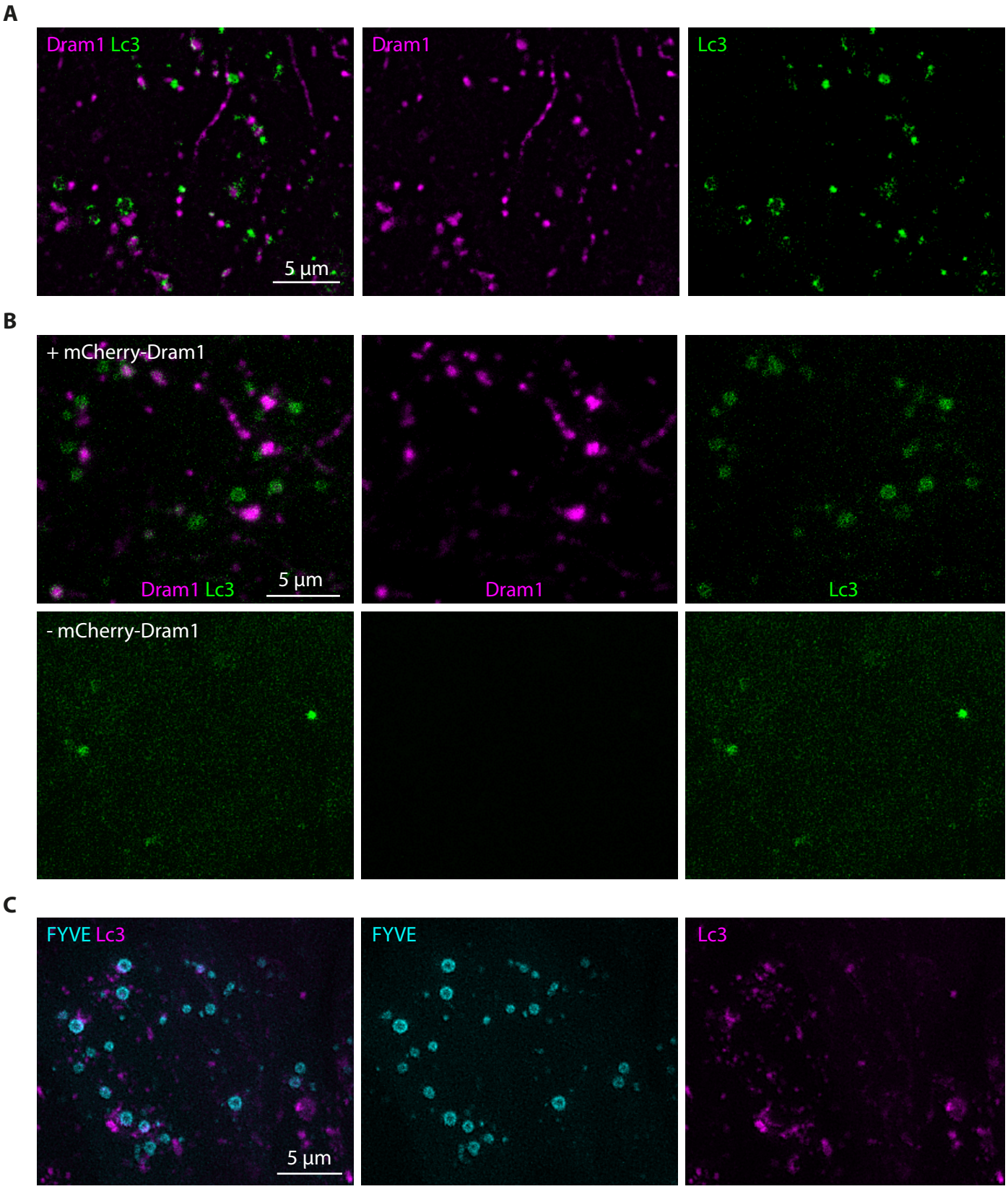

<Figure 2>

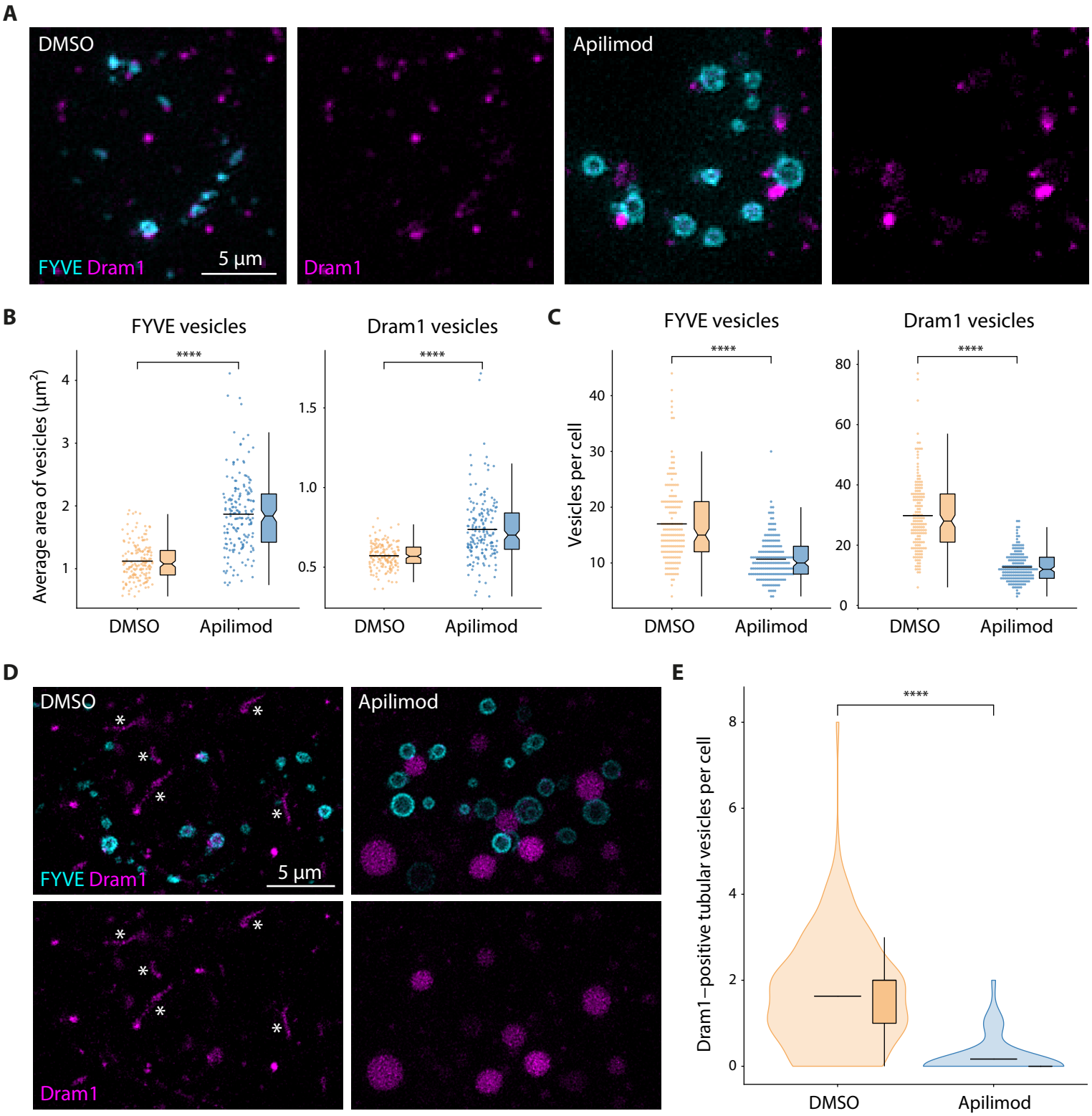
A
DMSO
FYVE Dram1
5 µm
Dram1
Apilimod
B
FYVE vesicles
Dram1 vesicles
Average area of vesicles (µm²)
****
DMSO
Apilimod
C
FYVE vesicles
Dram1 vesicles
Vesicles per cell
****
DMSO
Apilimod
D
DMSO
FYVE Dram1
5 µm
Apilimod
Dram1
E
Dram1−positive tubular vesicles per cell
****
DMSO
Apilimod

<Supplementary Figure 2>

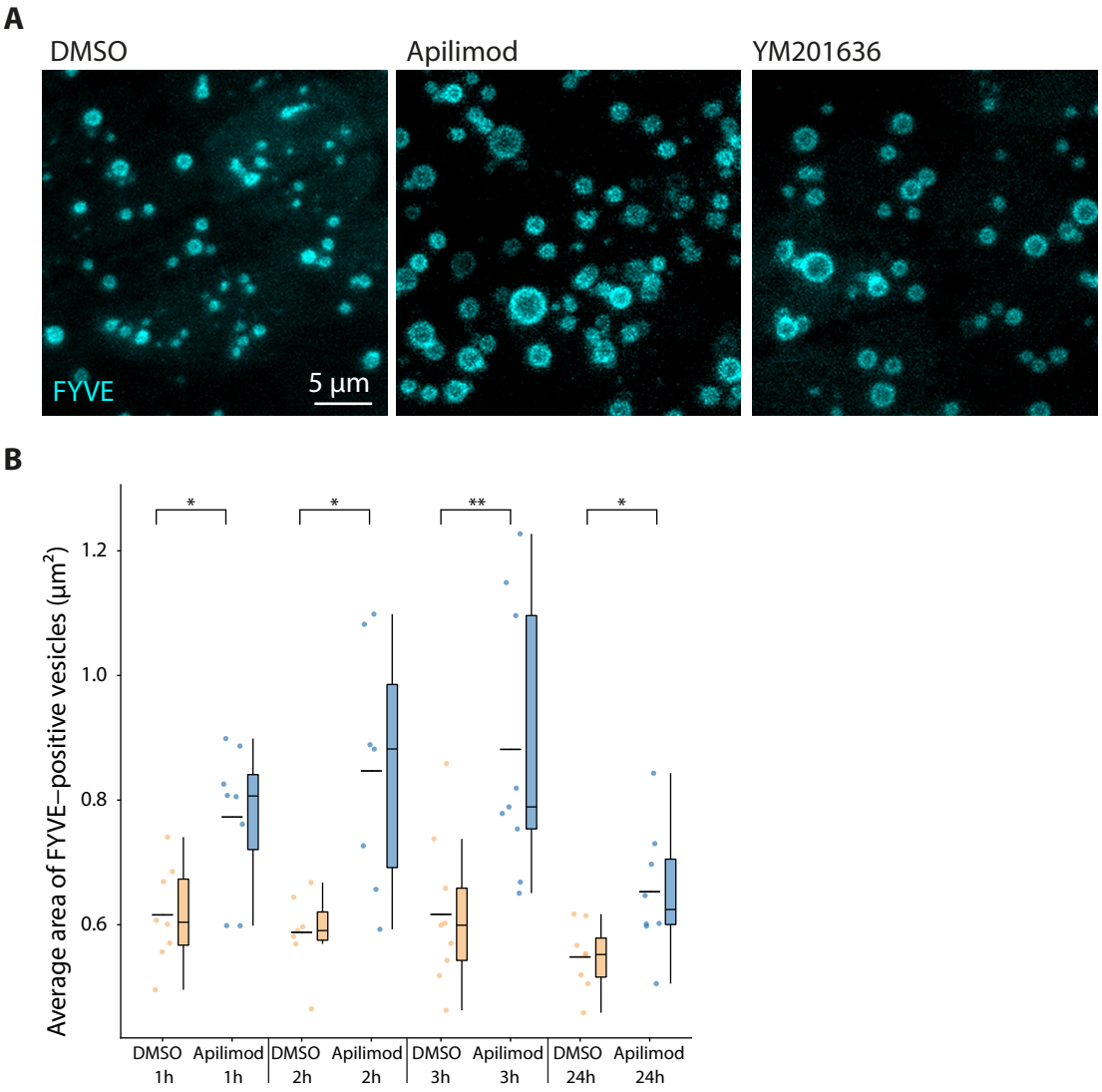

<Supplementary Figure 3>

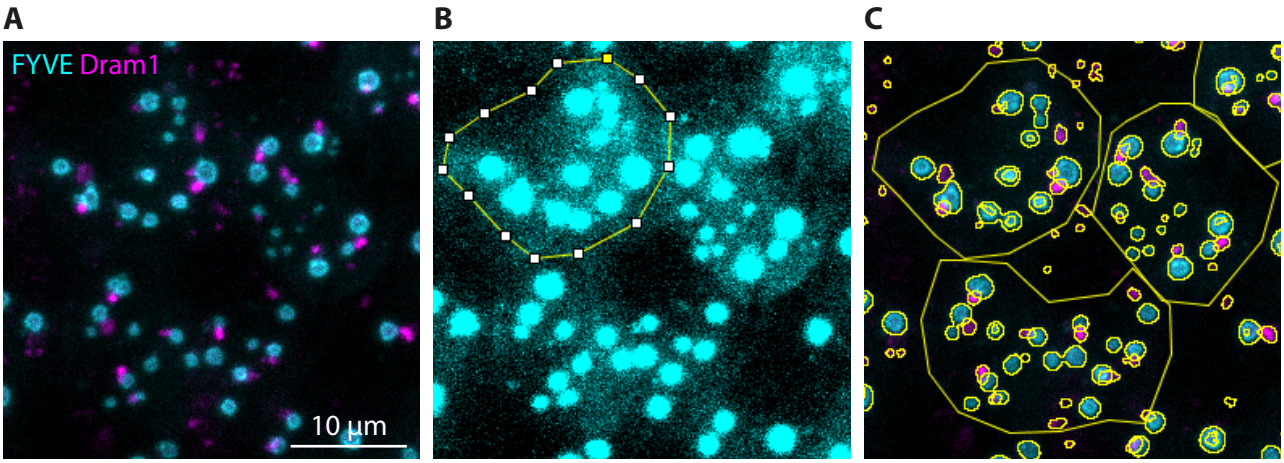

<Figure 3>

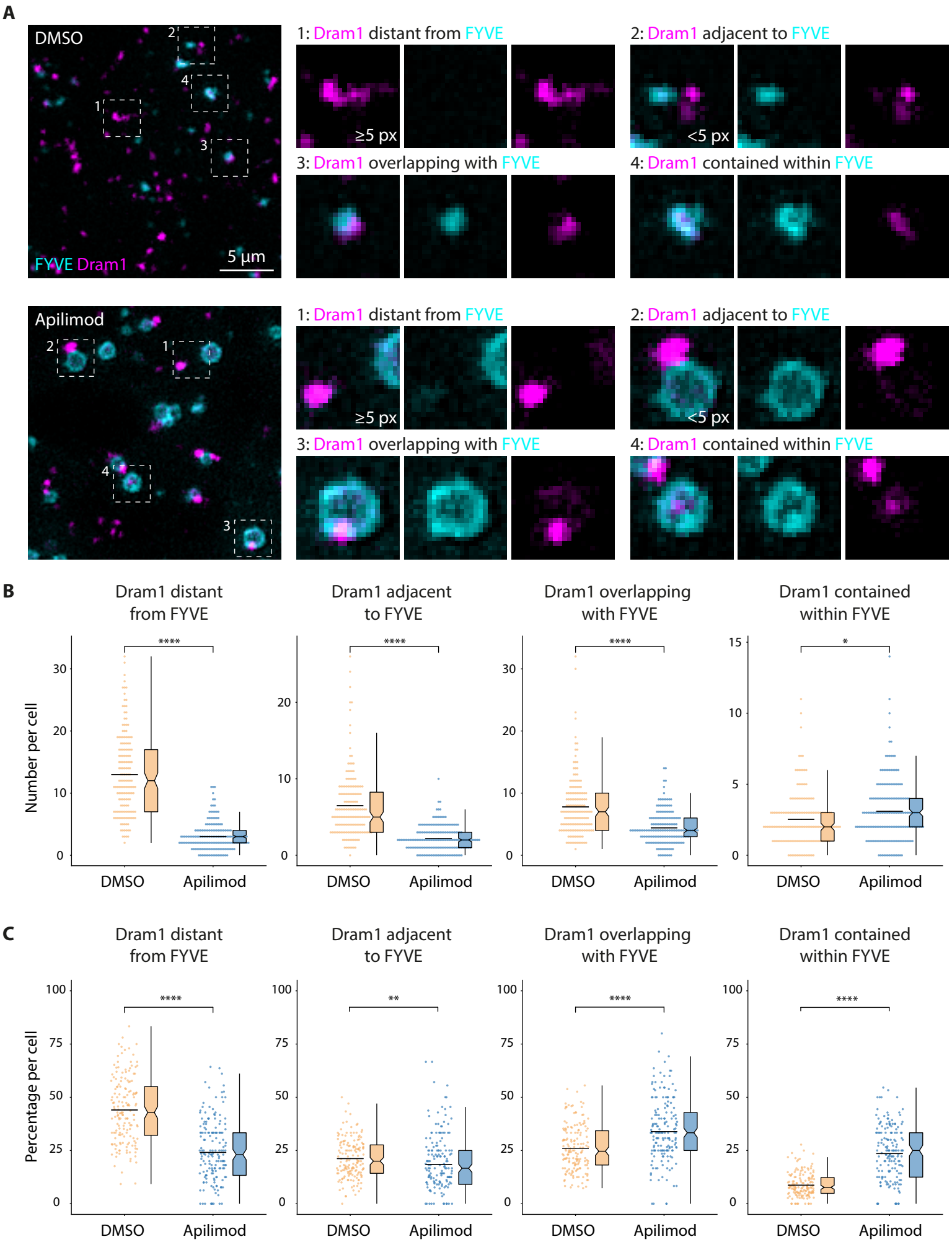
A
DMSO
FYVE Dram1
5 µm
1: Dram1 distant from FYVE
2: Dram1 adjacent to FYVE
3: Dram1 overlapping with FYVE
4: Dram1 contained within FYVE
≥5 px
<5 px
Apilimod
B
Dram1 distant from FYVE
Dram1 adjacent to FYVE
Dram1 overlapping with FYVE
Dram1 contained within FYVE
Number per cell
DMSO
Apilimod
C
Percentage per cell

<Figure 4>

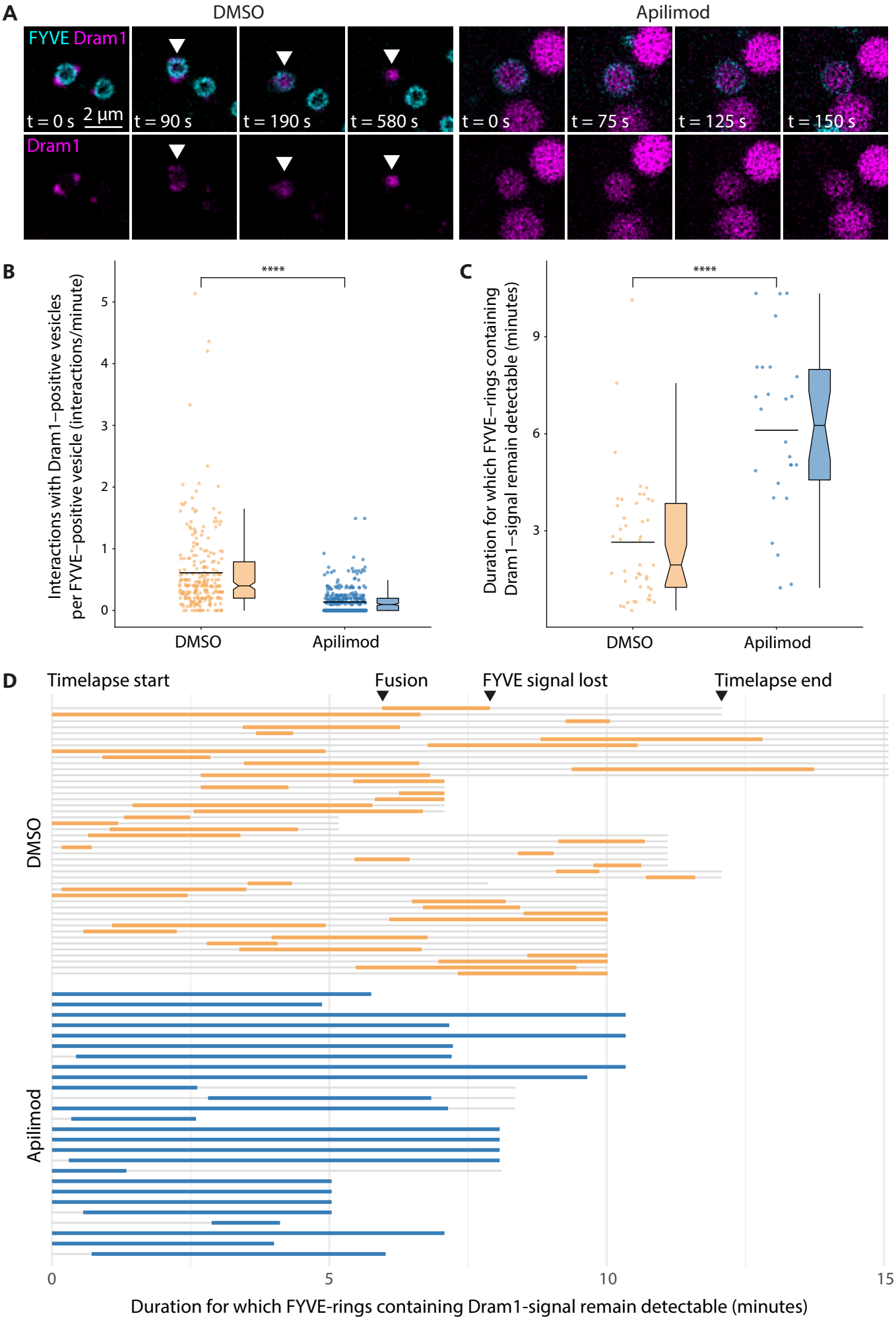
A
DMSO
Apilimod
FYVE Dram1
Dram1
t = 0 s
2 µm
t = 90 s
t = 190 s
t = 580 s
t = 0 s
t = 75 s
t = 125 s
t = 150 s
B
Interactions with Dram1−positive vesicles per FYVE−positive vesicle (interactions/minute)
****
DMSO
Apilimod
C
Duration for which FYVE−rings containing Dram1−signal remain detectable (minutes)
****
DMSO
Apilimod
D
Timelapse start
Fusion
FYVE signal lost
Timelapse end
DMSO
Apilimod
0
5
10
15
Duration for which FYVE-rings containing Dram1-signal remain detectable (minutes)

<Figure 5>

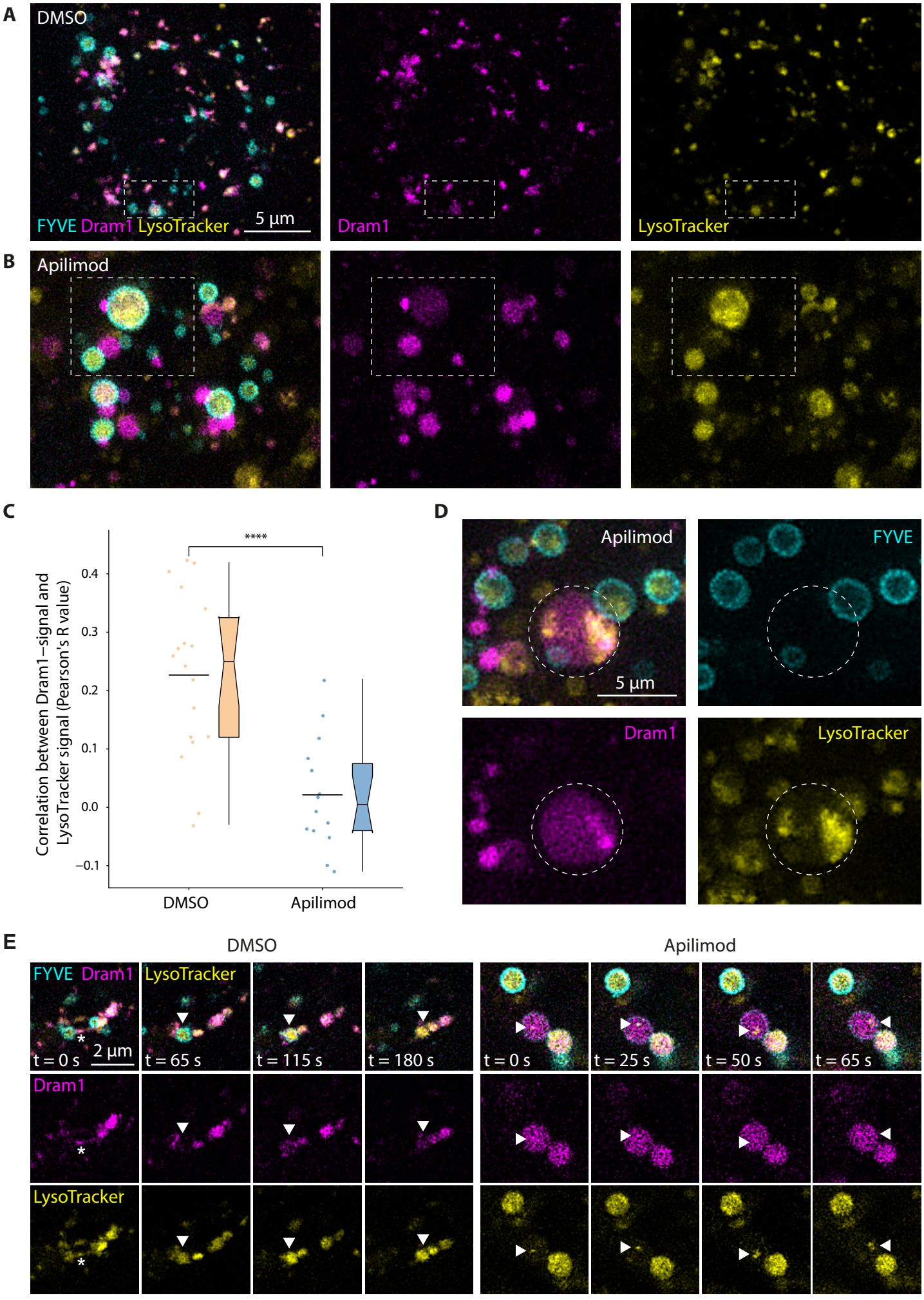
A
DMSO
FYVE Dram1 LysoTracker
5 µm
Dram1
LysoTracker
B
Apilimod
C
****
Correlation between Dram1−signal and LysoTracker signal (Pearson's R value)
0.4
0.3
0.2
0.1
0.0
−0.1
DMSO
Apilimod
D
Apilimod
5 µm
FYVE
Dram1
LysoTracker
E
DMSO
Apilimod
FYVE Dram1
LysoTracker
2 µm
t = 0 s
t = 65 s
t = 115 s
t = 180 s
t = 0 s
t = 25 s
t = 50 s
t = 65 s
Dram1
LysoTracker